Figure S1

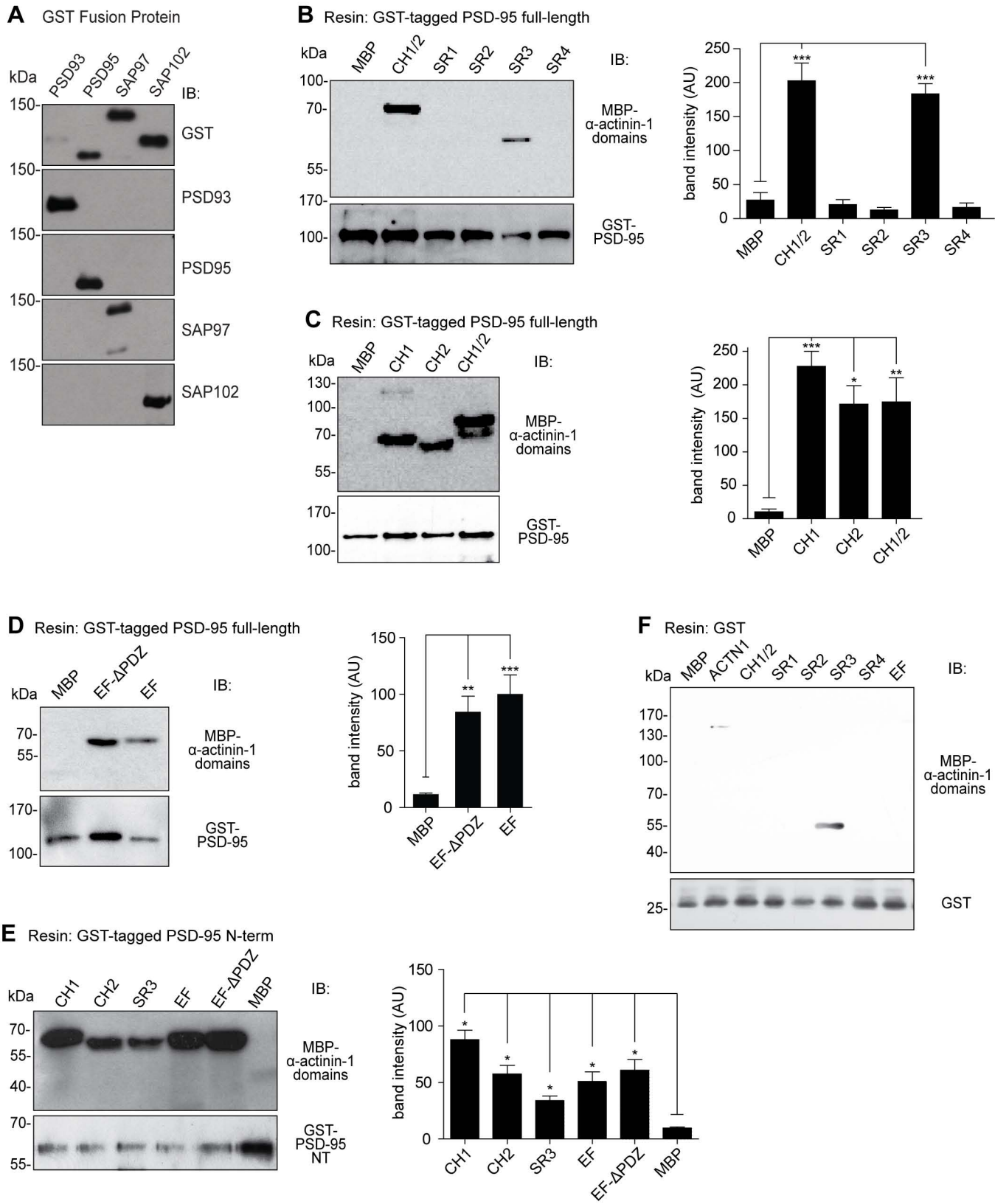
A
GST Fusion Protein
kDa
PSD93
PSD95
SAP97
SAP102
IB:
150-
GST
PSD93
PSD95
SAP97
SAP102
B
Resin: GST-tagged PSD-95 full-length
kDa
MBP
CH1/2
SR1
SR2
SR3
SR4
IB:
100-
70-
55-
170-
MBP-
α-actinin-1
domains
GST-
PSD-95
band intensity (AU)
250
200
150
100
50
0
***
***
C
Resin: GST-tagged PSD-95 full-length
kDa
MBP
CH1
CH2
CH1/2
IB:
130-
100-
70-
55-
170-
MBP-
α-actinin-1
domains
GST-
PSD-95
band intensity (AU)
***
*
**
D
Resin: GST-tagged PSD-95 full-length
kDa
MBP
EF-ΔPDZ
EF
IB:
70-
55-
170-
100-
MBP-
α-actinin-1
domains
GST-
PSD-95
band intensity (AU)
150
100
50
0
**
***
MBP
EF-ΔPDZ
EF
F
Resin: GST
kDa
MBP
ACTN1
CH1/2
SR1
SR2
SR3
SR4
EF
IB:
170-
130-
100-
70-
55-
40-
25-
MBP-
α-actinin-1
domains
GST
E
Resin: GST-tagged PSD-95 N-term
kDa
CH1
CH2
SR3
EF
EF-ΔPDZ
MBP
IB:
70-
55-
40-
MBP-
α-actinin-1
domains
GST-
PSD-95
NT
band intensity (AU)
150
100
50
0
*
CH1
CH2
SR3
EF
EF-ΔPDZ
MBP

Figure S1. Antibodies against PSD-93, PSD-95, SAP97, and SAP102 and interactions of full-length PSD-95 with α-actinin-1 CH1/2 and EF-hand domains but not with SR3 are specific, related to Figure 1.

(**A**) GST fusion proteins of PSD-93, PSD-95, SAP97 and SAP102 were expressed in *E. coli* and affinity purified on glutathione Sepharose before immunoblotting with antibodies against GST, PSD-93, PSD-95, SAP97 and SAP102. The amounts of loaded GST fusion proteins were adjusted over several trials so that immunosignals of individual bands with the individual antibodies resulted in comparable signal strength for each protein to compare their relative specificities except GST, which was used to illustrate the respective amount of protein loaded. Of note, much smaller amount of PSD-93 than of the other three proteins had to be loaded as reflected by the low signal with anti-GST (top) to obtain comparable signals indicating that the anti-PSD-93 antibody is much stronger for IB than the other three antibodies.

(**B**) Top: Pull-down of MBP-tagged α-actinin domains but not MBP alone by immobilized full-length PSD-95. Bottom: IB with anti-GST antibody indicates that comparable amounts of PSD-95 were present in all samples. Right: Densitometric MBP quantification (in AU: MBP: 27.1 ± 11.2; CH1/2: 202.8 ± 26.1; SR1: 20.6 ± 7.2; SR2: 12.6 ± 3.7; SR3: 183.5 ± 15.2; SR4: 16.4 0 ± 6.6).

(**C**) Top: Pull-down of MBP-tagged α-actinin CH1, CH2 and CH1/2 domains but not MBP alone by immobilized full-length PSD-95. Bottom IB with anti-GST antibody indicates comparable amounts of PSD-95 in all samples. Right: Densitometric quantification of MBP signals (in AU: MBP: 10.4 ± 4.3; CH1: 227.8 ± 22.3; CH2: 171.1 ± 27.6; CH1/2: 174.3 ± 36.23; n = 5).

(**D**) Top: Pull-down of MBP-tagged α-actinin EF-hand domain and EF-hand domain lacking the C-terminal PDZ ligand (EF-ΔPDZ) but not MBP alone by immobilized full-length PSD-95. Bottom: IB with anti-GST antibody indicates that comparable amounts of PSD-95 were present in all samples. Right: Densitometric quantification (in AU: MBP: 11.4 ± 1.3; EF-ΔPDZ: 84.3 ± 14.1; EF: 100 ± 17.3; n = 8).

(**E**) Top: Pull-down of MBP-tagged α-actinin domains but not MBP alone by immobilized PSD-95 residues 1-71 (PSD-95 N-term). Bottom: Comparable amounts of PSD-95 were present in all samples. Right: Densitometric quantification (in AU: CH1: 88.4 ± 9.6; CH2: 57.5 ± 7.3; SR3: 34.4 ± 4.0; EF: 51.4 ± 8.2; EF-ΔPDZ: 61.4 ± 9.6; MBP: 11.0 ± 1.1).

(**F**) Top: Pull-down of MBP-tagged full-length α-actinin and SR3 but none of the other α-actinin domains by immobilized GST. Bottom: Equal amounts of GST were present in all samples.

Statistical significance was tested by 1-way ANOVA with Dunnett's Multiple Comparison Test.

Figure S2

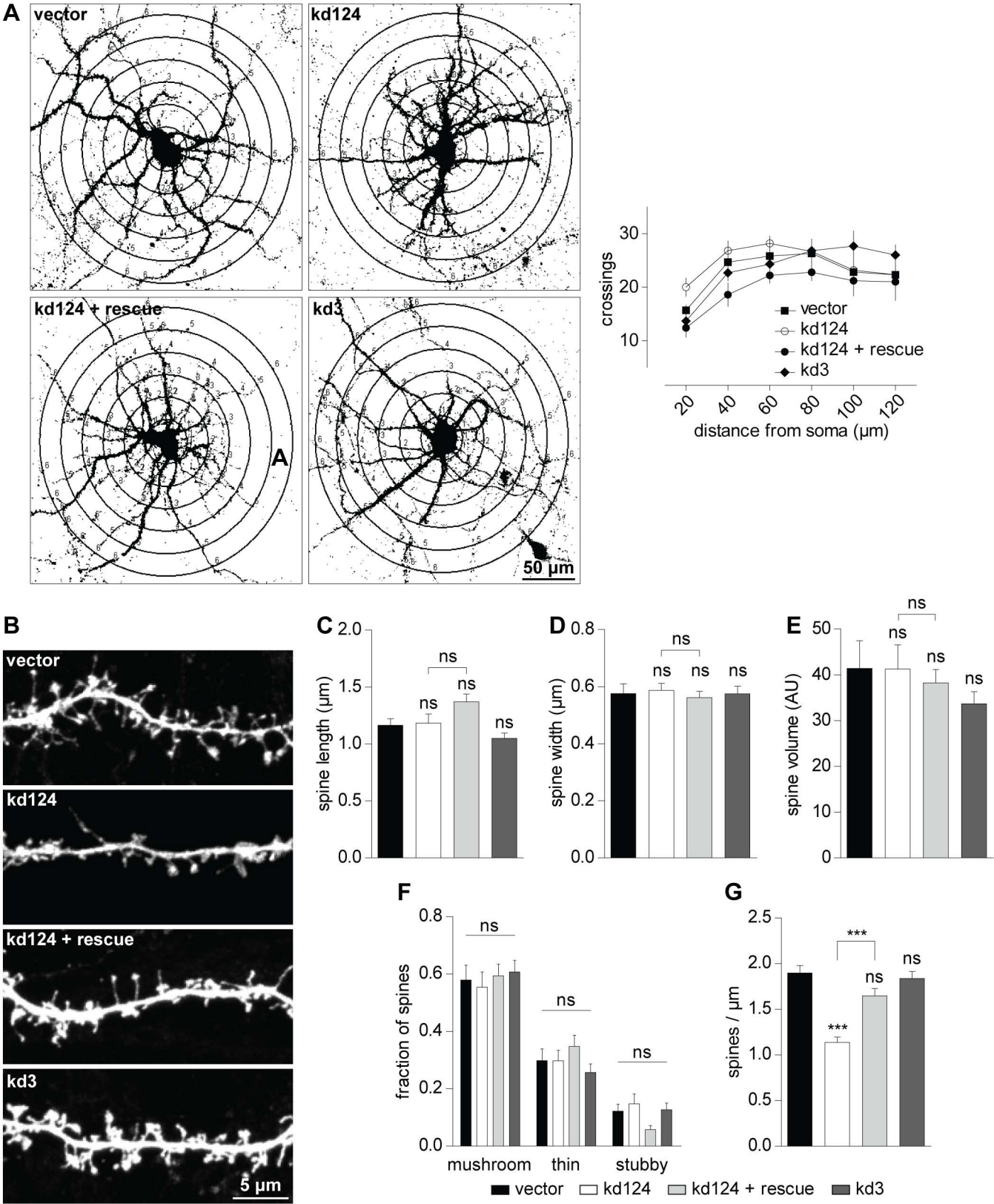
A
vector
kd124
kd124 + rescue
kd3
A
50 µm
crossings
30
20
10
vector
kd124
kd124 + rescue
kd3
20
40
60
80
100
120
distance from soma (µm)
B
vector
kd124
kd124 + rescue
kd3
5 µm
C
spine length (µm)
2.0
1.5
1.0
0.5
0.0
ns
ns
ns
ns
ns
D
spine width (µm)
0.8
0.6
0.4
0.2
0.0
ns
ns
ns
ns
E
spine volume (AU)
50
40
30
20
10
0
ns
ns
ns
ns
ns
F
fraction of spines
0.8
0.6
0.4
0.2
0.0
ns
ns
ns
mushroom
thin
stubby
G
spines / µm
2.5
2.0
1.5
1.0
0.5
0.0
***
***
ns
ns
vector
kd124
kd124 + rescue
kd3

Figure S2. Knockdown of α-actinin reduces spine density without influencing the morphology of dendrites and spines, related to Figure 2.

Primary embryonic rat hippocampal cultures were transfected at 4 DIV and fixed at 18 DIV. Parental pSilencer vector encoding eGFP from an independent promoter (vector) and shRNA against α-actinin-3 (kd3), which is not expressed in neurons, served as control. α-actinin-1, -2, and -4 were knocked-down with specific shRNAs (kd124; Hall et al., 2013; Schnizler et al., 2009) while shRNA-insenitive α-actinin-1* rescue was co-expressed (Hall et al., 2013).

(**A**) The number of dendrites crossing each concentric circle was not different for kd124 compared to vector, kd124 + rescue, as well as kd3. Images were taken at low magnification on an epifluorescence microscope and transformed into binary images using thresholding. Quantification in the right panel.

(**B-G**) Confocal Z-stacks of transfected cells were taken using a 100x objective lens (**B**). Individual Z-slices to measure spine length, width, and volume as well as to assess spine type (**C-F**), while maximum-intensity projections served to count spine density (**G**). For each analysis, the experimenter was blinded to the conditions.

(**C**) The length of individual spines is not altered after transfection with kd124, kd124 + rescue, or kd3 (in µm: vector: 1.17 ± 0.06; kd124: 1.18 ± 0.08; kd124 + rescue: 1.37 ± 0.07; kd3: 1.05 ± 0.05; n > 21 images from 4 independent experiments).

(**D**) Spine width is not altered by kd124, kd124 + rescue, or kd3 (in µm: vector: 0.58 ± 0.03; kd124: 0.59 ± 0.02; kd124 + rescue: 0.56 ± 0.02; kd3: 0.58 ± 0.03; n > 21 images from 4 independent experiments).

(**E**) Spine volume is not changed by kd124, kd124 + rescue, or kd3 (in AU: vector: 41.4 ± 6.0; kd124: 41.3 ± 5.2; kde124 + rescue: 38.2 ± 2.9; kd3: 33.7 ± 2.7; n > 21 images from 4 independent experiments).

(**F**) Expression of kd124, kd124 + rescue, or kd3 did not influence the overall distribution of spine types in transfected neurons (mushroom (m), thin (t), stubby (s): vector: m: 0.58 ± 0.05, t: 0.30 ± 0.04, s: 0.12 ± 0.02; kd124: m: 0.55 ± 0.05, t: 0.30 ± 0.04, s: 0.15 ± 0.03; kd124 + rescue: m: 0.60 ± 0.04, t: 0.35 ± 0.04, s: 0.05 ± 0.01; kd3: m: 0.61 ± 0.04, t: 0.26 ± 0.03, s: 0.13 ± 0.02; n > 21 images from 4 independent experiments).

(**G**) The spine density is significantly reduced by kd124, but not by kd124 + rescue or kd3 (in μm^{-1}: vector; 1.90 ± 0.08; kd124: 1.14 ± 0.06; kd124 + rescue: 1.65 ± 0.08; kd3: 1.84 ± 0.08; n > 45 images from > 22 cells from 5 independent experiments).

Statistical significance was tested by 1-way ANOVA with Bonferroni's Multiple Comparison Test.

Figure S3

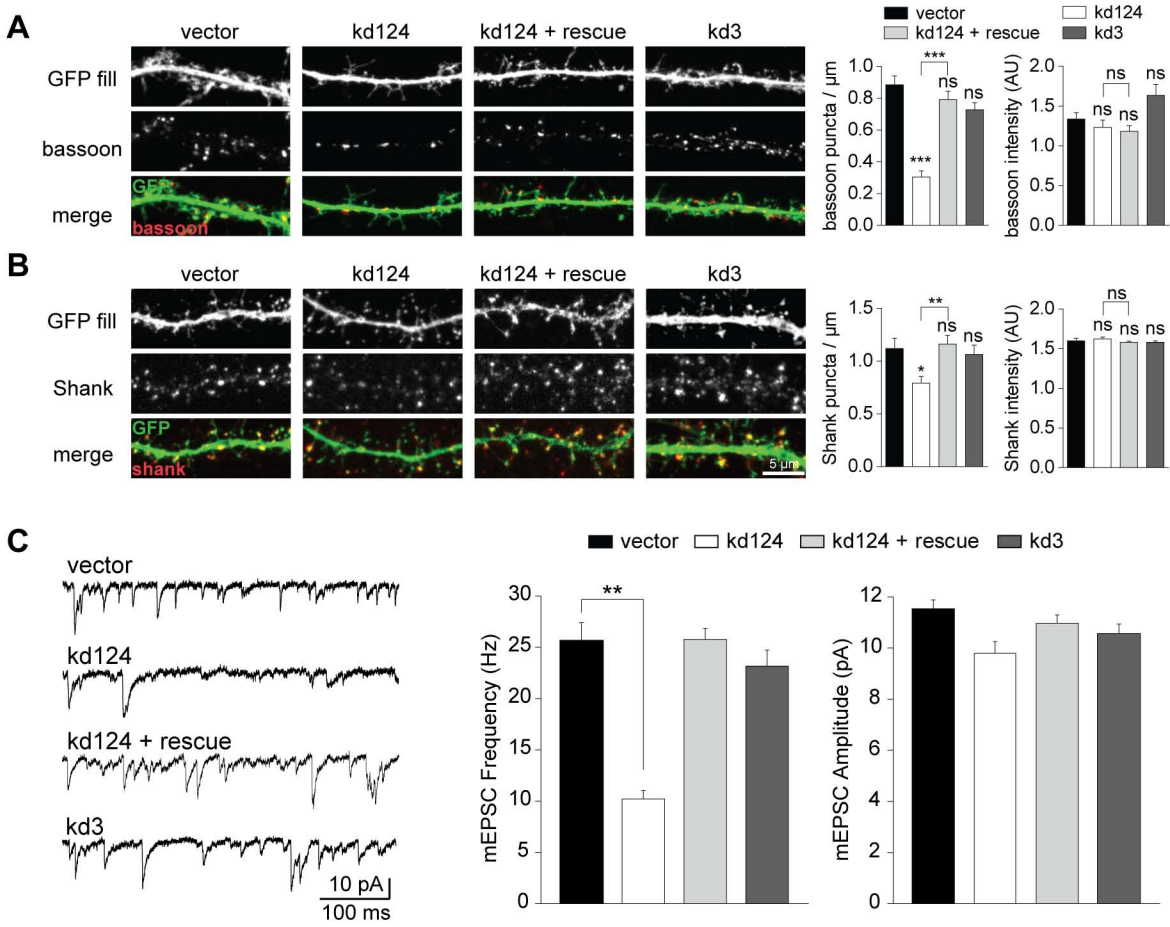
A
vector
kd124
kd124 + rescue
kd3
GFP fill
bassoon
merge
GFP
bassoon
vector
kd124
kd124 + rescue
kd3
bassoon puncta / µm
bassoon intensity (AU)
***
ns
B
Shank
shank
Shank puncta / µm
Shank intensity (AU)
*
**
5 µm
C
mEPSC Frequency (Hz)
mEPSC Amplitude (pA)
10 pA
100 ms

Figure S3. α-actinin kd reduces density but not intensity of bassoon and Shank IF puncta and reduces mEPSC frequency but not amplitude, related to Figure 2.

Hippocampal cultures were transfected and fixed as in Figure 4. Cells were used for whole-cell patch-clamp experiments at DIV 11-14 or fixed and stained at 18 DIV

(**A**) Puncta density of bassoon was significantly reduced by kd124 but not by kd124 + rescue or kd3 (in μm^{-1}: vector: 0.88 ± 0.06; kd124: 0.31 ± 0.04; kd124 + rescue: 0.79 ± 0.05; kd3: 0.72 ± 0.05). Puncta intensity was not affected (in AU: vector: 1.34 ± 0.08; kd124: 1.23 ± 0.09; kd124 + rescue: 1.2 ± 0.07; kd3: 1.63 ± 0.14; n > 53 images from > 26 cells from 5 independent experiments).

(**B**) Puncta density of Shank was reduced by kd124 but not by kd124 + rescue or kd3 (in μm^{-1}: vector: 1.12 ± 0.10; kd124: 0.79 ± 0.06; kd124 + rescue: 1.16 ± 0.08; kd3: 1.06 ± 0.09). Puncta intensity was not affected (in AU: vector: 1.60 ± 0.03; kd124: 1.62 ± 0.02; kd124 + rescue: 1.58 ± 0.02; kd3: 1.58 ± 0.02; n > 34 images from > 17 cells from 3 independent experiments).

(**C, D**) mEPSC frequency was significantly reduced by kd124 but not by kd124 + rescue or kd3 (in Hz: vector: 25.7 ± 1.8; kd124: 10.2 ± 0.8; kd124 + rescue: 25.7 ± 1.1; kd3: 23.1 ± 1.6). mEPSC amplitude was not altered by either kd or co-expression of rescue (in pA: vector: 11.5 ± 0.3; kd124: 9.8 ± 0.4; kd124 + rescue: 11.0 ± 0.3; kd3: 10.5 ± 0.4).

Statistical significance was tested by 1-way ANOVA with Bonferroni's Multiple Comparison Test.

Figure S4

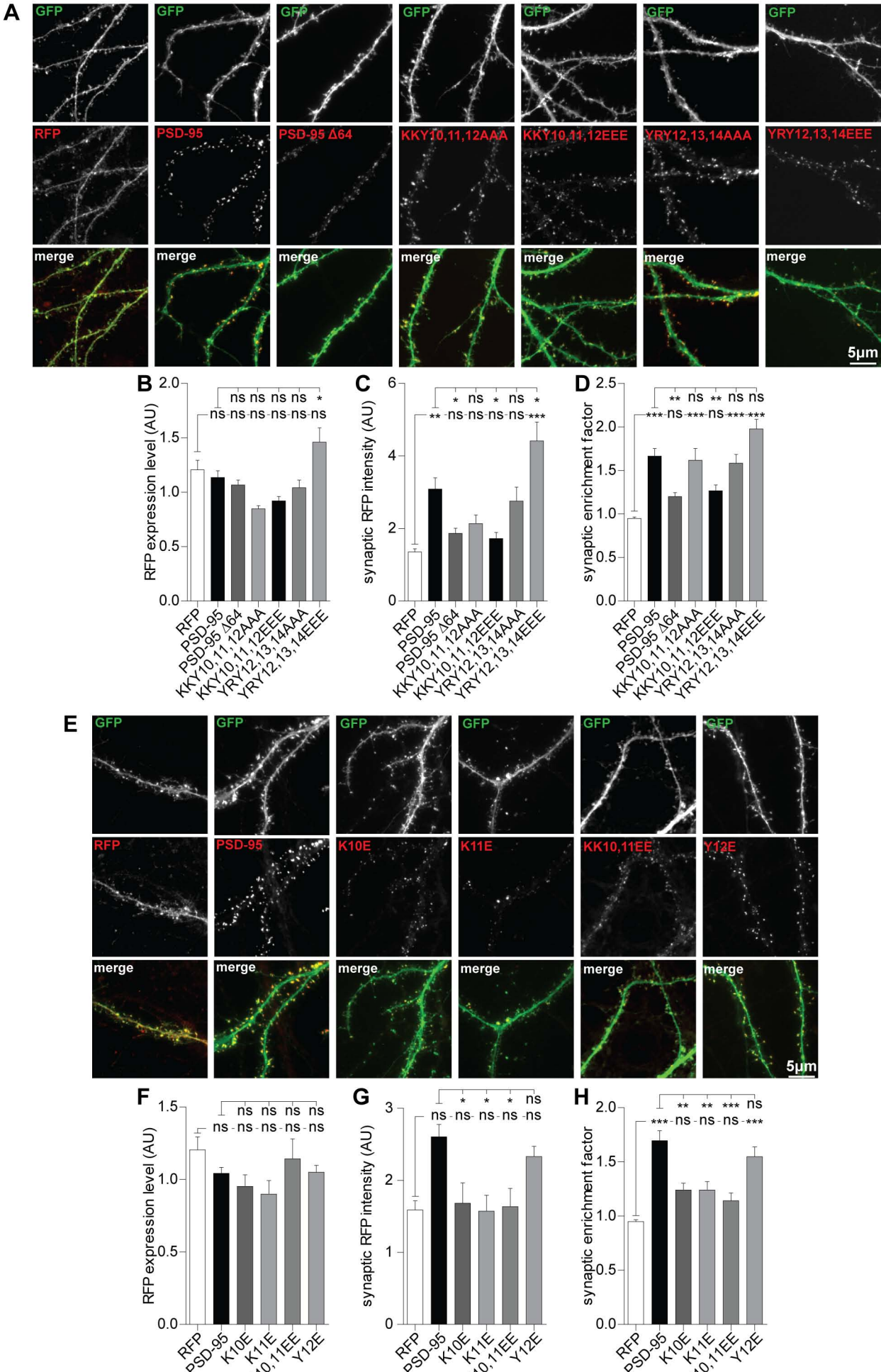
A
GFP
RFP
PSD-95
PSD-95 Δ64
KKY10,11,12AAA
KKY10,11,12EEE
YRY12,13,14AAA
YRY12,13,14EEE
merge
5μm
B
RFP expression level (AU)
C
synaptic RFP intensity (AU)
D
synaptic enrichment factor
RFP
PSD-95
PSD-95 Δ64
KKY10,11,12AAA
KKY10,11,12EEE
YRY12,13,14AAA
YRY12,13,14EEE
E
K10E
K11E
KK10,11EE
Y12E
F
G
H
PSD-95
K10E
K11E
KK10,11EE
Y12E

Figure S4. Role of PSD-95 N-terminus and residues 10-14 in synaptic targeting of PSD-95, related to Figure 4.

Hippocampal cultures were transfected at 7 DIV with GFP as cell-fill and RFP-tagged PSD-95, fixed at 18 DIV and imaged by epifluorescence microscopy with a 100x objective lens.

(**A**) Representative images of cells transfected with PSD-95^{WT}, PSD-95 Δ64, PSD-95^{KKY10,11,12EEE}, PSD-95^{KKY10,11,12AAA}, PSD-95^{YRY12,13,14AAA}, PSD-95^{YRY12,13,14EEE}.

(**B**) Expression levels were comparable between all the mutated constructs in (**A**) with the exception of PSD-95^{YRY12,13,14EEE} which showed slightly higher expression as estimated by cell-wide RFP fluorescence intensity normalized to cell-wide GFP fluorescence intensity (in AU: RFP: 1.21 ± 0.09; PSD-95^{WT}: 1.14 ± 0.06; PSD-95 Δ64: 1.07 ± 0.04; PSD-95^{KKY10,11,12AAA}: 0.85 ± 0.03; PSD-95^{KKY10,11,12EEE}: 0.92 ± 0.04; PSD-95^{YRY12,13,14AAA}: 1.04 ± 0.07; PSD-95^{YRY12,13,14EEE}: 1.46 ± 0.13).

(**C**) Synaptic RFP intensity in spines normalized to cell-wide GFP intensity was significantly increased vs RFP only for PSD-95^{WT} and PSD-95^{YRY12,13,14EEE}. (in AU: RFP: 1.35 ± 0.09; PSD-95^{WT}: 3.09 ± 0.31; PSD-95 Δ64: 1.86 ± 0.14; PSD-95^{KKY10,11,12AAA}: 2.14 ± 0.23; PSD-95^{KKY10,11,12EEE}: 1.72 ± 0.17; PSD-95^{YRY12,13,14AAA}: 2.76 ± 0.39; PSD-95^{YRY12,13,14EEE}: 4.42 ± 0.52).

(**D**) Synaptic enrichment was significantly increased vs RFP for all PSD-95 constructs except PSD-95 Δ64 and PSD-95^{YRY10,11,12EEE}. (RFP: 0.95 ± 0.02; PSD-95^{WT}: 1.67 ± 0.09; PSD-95 Δ64: 1.20 ± 0.04; PSD-95^{KKY10,11,12AAA}: 1.62 ± 0.13; PSD-95^{KKY10,11,12EEE}: 1.27 ± 0.07; PSD-95^{YRY12,13,14AAA}: 1.58 ± 0.10; PSD-95^{YRY12,13,14EEE}: 1.98 ± 0.11).

(**B-D**) n>19 images from > 9 cells from 3 independent experiments.

(**E**) Representative images of cells transfected with PSD-95^{WT}, PSD-95^{K10E}, PSD-95^{K11E} PSD-95^{KK10,11EE}, and PSD-95^{Y12E}

(**F**) Expression levels were comparable between all constructs in (**E**) (in AU: RFP: 1.21 ± 0.09; PSD-95^{WT}: 1.04 ± 0.04; PSD-95^{K10E}: 0.95 ± 0.08; PSD-95^{K11E}: 0.90 ± 0.09; PSD-95^{KK10,11EE}: 1.14 ± 0.14; PSD-95^{Y12E}: 1.05 ± 0.05).

(**G**) Synaptic RFP intensity in spines normalized to cell-wide GFP intensity was significantly increases vs RFP only for PSD-95^{WT} (in AU: RFP: 1.59 ± 0.13; PSD-95^{WT}: 2.60 ± 0.17; PSD-95^{K10E}: 1.68 ± 0.; PSD-95^{K11E}: 1.57 ± 0.22; PSD-95^{KK10,11EE}: 1.64 ± 0.25; PSD-95^{Y12E}: 2.33 ± 0.14).

(**H**) Synaptic enrichment was significantly increased vs RFP only for PSD-95^{WT} and PSD-95^{Y12E} (in AU: RFP: 0.94 ± 0.03; PSD-95^{WT}: 1.70 ± 0.09; PSD-95^{K10E}: 1.24 ± 0.06; PSD-95^{K11E}: 1.24 ± 0.08; PSD-95^{KK10,11EE}: 1.14 ± 0.07; PSD-95^{Y12E}: 1.55 ± 0.09).

(**F-H**) n>18 images from > 9 cells from 3 independent experiments.

Statistical significance was tested by 1-way ANOVA with Bonferroni's Multiple Comparison Test.

Figure S5

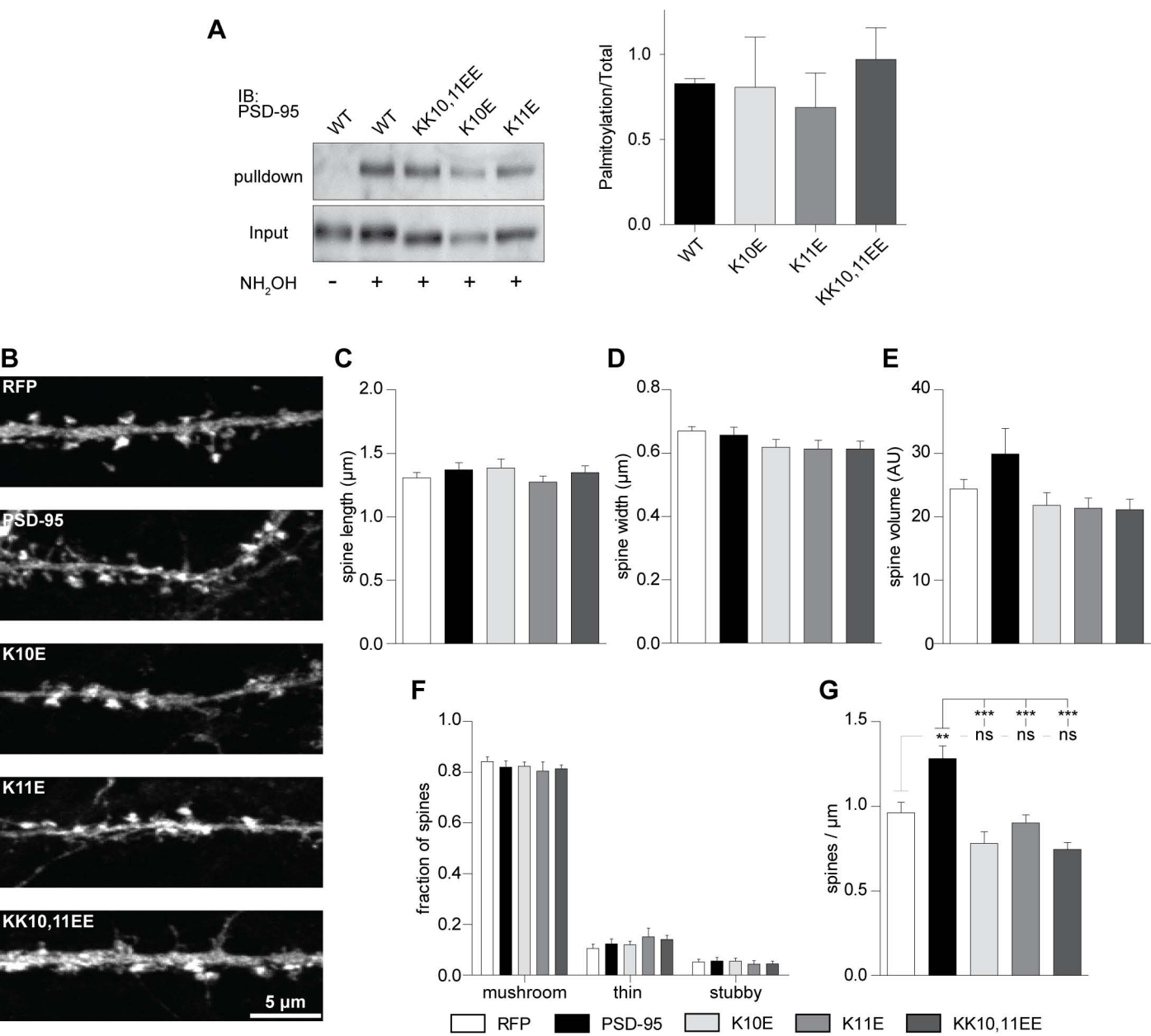
A
IB:
PSD-95
WT
WT
KK10,11EE
K10E
K11E
pulldown
Input
NH2OH
- + + + +
Palmitoylation/Total
1.0
0.5
0.0
WT
K10E
K11E
KK10,11EE
B
RFP
PSD-95
K10E
K11E
KK10,11EE
5 µm
C
spine length (µm)
2.0
1.5
1.0
0.5
0.0
D
spine width (µm)
0.8
0.6
0.4
0.2
0.0
E
spine volume (AU)
40
30
20
10
0
F
fraction of spines
1.0
0.8
0.6
0.4
0.2
0.0
mushroom
thin
stubby
G
spines / µm
1.5
1.0
0.5
0.0
** ns ns ns
*** *** ***
RFP
PSD-95
K10E
K11E
KK10,11EE

Figure S5. Spine morphology and PSD-95 palmitoylation levels were unaltered but spine density was reduced after overexpression of PSD-95 mutants, related to Figure 5.

(**A**) HEK293T cells were transfected with RFP-tagged PSD-95^{WT}, PSD-95^{K10E}, PSD-95^{K11E}, and PSD-95^{KK10,11EE}. After 24h cells were lysed and free thiols alkylated with NEM. Palmitoyl-Cysteine thioesters were hydrolysed with NH_2OH before freed thiols were biotinylated. NeutrAvidin was used to pull-down biotinylated proteins followed by immunoblotting for PSD-95. Palmitoylation levels of PSD-95 mutants were not different from the wild-type. Omission of NH_2OH prevented pull-down proving the specificity of the procedure (left lane). The left panel shows a representative immunoblot, the right panel densitometric quantification (PSD-95^{WT}: 0.83 ± 0.03; PSD-95^{K10E}: 0.81 ± 0.29; PSD-95^{K11E}: 0.69 ± 0.20; PSD-95^{KK10,11EE}: 0.97 ± 0.19; n = 3).

(**B-G**) Primary embryonic rat hippocampal cultures were transfected at 7 DIV with GFP as cell-fill and RFP-tagged PSD-95 mutations. Cells were fixed at 18 DIV.

(**B**) Z-stacks were taken with a confocal laser-scanning microscope with 100x objective lens. Individual Z-slices were used for measuring spine length, width, and volume as well as to assess spine type (**C-F**). Maximum-intensity projections were used to count spine density (**G**). For each analysis, the experimenter was blinded to the conditions.

(**C**) Spine length was not altered by any PSD-95 mutant vs RFP alone or PSD-95^{WT} (in µm: RFP: 1.31 ± 0.04; PSD-95^{WT}: 1.37 ± 0.06; PSD-95^{K10E}: 1.38 ± 0.07; PSD-95^{K11E}: 1.27 ± 0.05; PSD-95^{KK10,11EE}: 1.35 ± 0.05).

(**D**) Spine width was not altered by any of the PSD-95 mutants vs RFP or PSD-95^{WT} (in µm: RFP: 0.67 ± 0.01; PSD-95^{WT}: 0.66 ± 0.03; PSD-95^{K10E}: 0.62 ± 0.03; PSD-95^{K11E}: 0.61 ± 0.02; PSD-95^{KK10,11EE}: 0.61 ± 0.02).

(**E**) Spine volume was not altered by any of the PSD-95 mutants vs RFP or PSD-95^{WT} (in AU: RFP: 24.4 ± 1.5; PSD-95^{WT}: 29.9 ± 4.0; PSD-95^{K10E}: 21.8 ± 2.0; PSD-95^{K11E}: 21.3 ± 1.6; PSD-95^{KK10,11EE}: 21.1 ± 1.7; n > 22 images from > 11 cells from 3 independent experiments).

(**F**) Spine type distribution is the same for all examined conditions (mushroom (m), thin (t), stubby (s): RFP: m: 0.84 ± 0.02, t: 0.11 ± 0.02, s: 0.05 ± 0.01; PSD-95: m: 0.82 ± 0.02, t: 0.12 ± 0.02, s: 0.06 ± 0.01; K10E: m: 0.82 ± 0.02, t: 0.12 ± 0.01, s: 0.06 ± 0.01; K11E: m: 0.80 ± 0.04, t: 0.15 ± 0.03, s: 0.04 ± 0.01; KK10,11EE: m: 0.81 ± 0.01, t: 0.14 ± 0.02, s: 0.04 ± 0.01).

(**G**) Spine density was significantly increased by PSD-95^{WT} but not PSD-95 mutants vs RFP. All PSD-95 mutants had significantly lower spine density than PSD-95^{WT} (in µm^{-1}: RFP: 0.96 ± 0.06; PSD-95^{WT}: 1.28 ± 0.07; PSD-95^{K10E}: 0.78 ± 0.07; PSD-95^{K11E}: 0.90 ± 0.05; PSD-95^{KK10,11EE}: 0.75 ± 0.04; n > 8 images from > 8 cells from 2 independent experiments).

Statistical significance was tested by 1-way ANOVA with Dunnett's (A) or Bonferroni's Multiple Comparison Test (C-G).

Figure S6

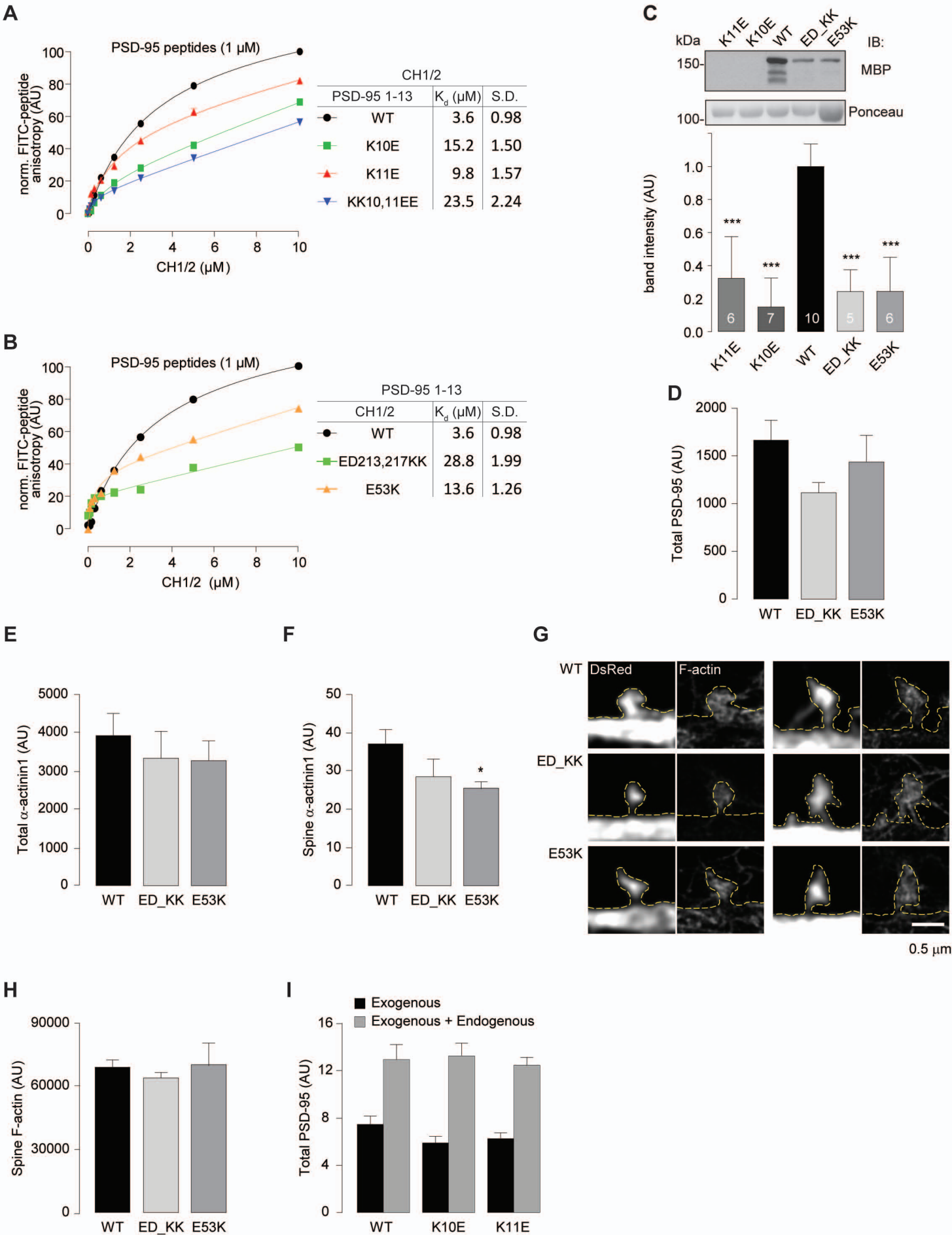
A
PSD-95 peptides (1 μM)
norm. FITC-peptide anisotropy (AU)
CH1/2 (μM)
CH1/2
PSD-95 1-13 | Kd (μM) | S.D.
WT 3.6 0.98
K10E 15.2 1.50
K11E 9.8 1.57
KK10,11EE 23.5 2.24
B
PSD-95 peptides (1 μM)
norm. FITC-peptide anisotropy (AU)
CH1/2 (μM)
PSD-95 1-13
CH1/2 | Kd (μM) | S.D.
WT 3.6 0.98
ED213,217KK 28.8 1.99
E53K 13.6 1.26
C
kDa
K11E
K10E
WT
ED_KK
E53K
IB:
150-
MBP
100-
Ponceau
band intensity (AU)
***
6
7
10
5
6
D
Total PSD-95 (AU)
WT
ED_KK
E53K
E
Total α-actinin1 (AU)
WT
ED_KK
E53K
F
Spine α-actinin1 (AU)
*
WT
ED_KK
E53K
G
WT
DsRed
F-actin
ED_KK
E53K
0.5 μm
H
Spine F-actin (AU)
WT
ED_KK
E53K
I
Exogenous
Exogenous + Endogenous
Total PSD-95 (AU)
WT
K10E
K11E

Figure S6. Mutation of K10 and K11 on PSD-95 as well as E213 and D217 on α-actinin-1 disrupts PSD-95 – α-actinin interaction but not F-actin content of spines, related to Figure 6.

(**A,B**) FP titration of N-terminally FITC-labeled peptides corresponding to residues 1-13 of PSD-95 (either with WT sequence or K10, K11, or both mutated to glutamate) with WT MBP-CH1-CH2 (**A**) or of PSD-95 1-13^{WT} with MBP-CH1-CH2^{WT}, MBP-CH1-CH2$^{ED213/217KK}$, or MBP-CH1-CH2^{E53K} (**B**). Titration curves are shown in the left panels; K_d-values for each interaction are given in the tables on the right. Every point corresponds to the average of 3 experiments.

Titration with CH1/2^{WT} showed reduced binding for all three mutated peptides.

(**C**) Full length GST-PSD-95^{WT}, PSD-95^{K10E}, and PSD-95^{K11E} were expressed in *E. coli* and comparable amounts immobilized as confirmed by Ponceau S-staining after transfer of gels (lower panel). Resins were incubated with equal amounts of full length MBP-α-actinin-1^{WT}, MBP-α-actinin-1^{E53K}, or MBP-α-actinin-1$^{ED213/217KK}$. Compared to pull down of MBP-α-actinin-1^{WT} with GST-PSD-95^{WT}, pull down of MBP-α-actinin-1$^{ED213/217KK}$ and of α-actinin-1^{E53K} with GST-PSD-95^{WT} was strongly reduced and pull down of MBP-α-actinin-1^{WT} with GST-PSD-95^{K10E} and GST-PSD-95^{K11E} nearly absent in this experiment. Bar diagram (bottom) indicates averaged band intensities (in AU: GST-PSD-95^{K10E} with MBP-α-actinin-1^{WT}: 0.32 ± 0.10 (n = 6); GST-PSD-95^{K11E} with MBP-α-actinin-1^{WT}: 0.15 ± 0.07 (n = 7); GST-PSD-95^{WT} with MBP-α-actinin-1^{WT}: 1.0 ± 0.04 (n = 10); GST-PSD-95^{WT} with MBP-α-actinin-1$^{ED213/217KK}$: 0.24 ± 0.06 (n = 5); GST-PSD-95^{WT} with MBP-α-actinin-1^{E53K}: 0.24 ± 0.08 (n = 6). From 10 different experiments.

(**D-H**) Hippocampal cultures were transfected at 7 DIV with α-actinin kd124 plasmids and sh-RNA resistant plasmids for replacement of endogenous α-actinin by α-actinin-1*^{WT}, α-actinin-1*^{E53K}, or α-actinin-1*^{ED213,217KK}.

(**D**) Total PSD-95 levels as determined in dendritic areas including shaft and spines by IF signals with anti-PSD-95 antibody were comparable for neurons expressing α-actinin-1^{WT}, α-actinin-1^{E53K}, and α-actinin-1$^{ED213/217KK}$ (in AU: WT: 1678.03 ± 205.05 (n=22 cells); ED213/217KK (ED_KK): 1084.42 ± 107.37 (n=11); E53K: 1447.60 ± 277.31 (n=16); from 2 independent experiments).

(**E**) Total α-actinin-1 levels as determined in dendritic areas including shaft and spines by IF signals with α-actinin-1 antibody were comparable for neurons expressing α-actinin-1^{WT}, α-actinin-1^{E53K}, and α-actinin-1$^{ED213/217KK}$ (in AU: WT: 3908.12 ± 589.86 (n=22 cells); ED_KK: 3319.60 ± 705.79 (n=11); E53K: 3274.27 ± 503.14 (n=16); from 2 independent experiments).

(**F**) α-actinin-1 levels as determined in spines by IF signals with α-actinin-1 antibody were statistically significantly lower for neurons expressing α-actinin-1^{E53K} (but not α-actinin-1$^{ED213/217KK}$) vs α-actinin-1^{WT} (in AU: WT: 36.92 ± 3.89 (n=22 cells); ED_KK: 28.58 ± 4.52 (n=11); E53K: 25.39 ± 1.79 (n=16); from 2 independent experiments).

(**G**) Sample images of F-actin in spines. DsRed expressed from the shRNA vectors (pSilencer) was used to visualize spine shape in the confocal microscopy mode. F-actin was imaged using Alexa488-conjugated phalloidin in STED microscopy mode.

(**H**) F-actin levels in spines were comparable for neurons expressing α-actinin-1^{WT}, α-actinin-1^{E53K}, and α-actinin-1$^{ED213/217KK}$ (in AU: WT: 69095.09 ± 3056.02 (n=15 cells); ED_KK: 63951.24 ± 2445.52 (n=21); E53K: 70493.01 ± 9642.24 (n=13); from 6 independent experiments).

(**I,J**) Hippocampal cultures were infected with a virus carrying shRNA to knock down endogenous PSD-95 and sh-resistant cDNA for ectopic expression of GFP-PSD-95* (Schluter et al., 2006).

(**I**) Total PSD-95 levels as determined in dendritic areas including shaft and spines by IF signals with anti-PSD-95 antibody (grey bars) as well as total levels of ectopically expressed GFP-PSD-95 as determined by GFP signals (black bars) were comparable for neurons expressing GFP-PSD-95^{WT}, GFP-PSD-95^{K10E}, and GFP-PSD-95^{K11E} (in AU: exogenous PSD-95: WT: 7.34 ± 0.63 (n=19 cells); K10E: 5.87 ± 0.59 (n=20 cells); K11E: 6.40 ± 0.36 (n=21 cells); exogenous + endogenous PSD-95: WT:12.92 ± 1.16 (n=19 cells); K10E: 13.22 ± 1.13 (n=20 cells); K11E: 12.76 ± 0.69 (n=21 cells); from 2 independent experiments)

Statistical significance was tested by 1-way ANOVA with Bonferroni's Multiple Comparison Test (C) or Kruskal-Wallis test followed by Mann-Whitney U test with Bonferroni correction (D-F, H and J).

Figure S7

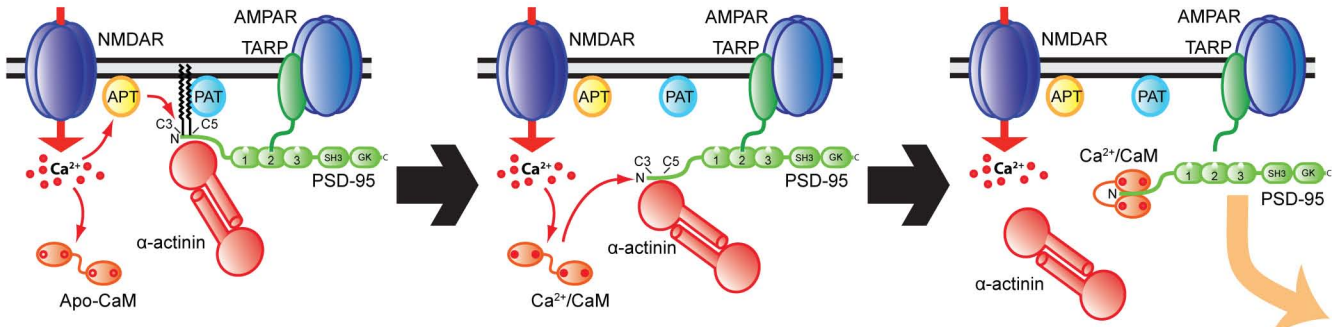
NMDAR
AMPAR
TARP
APT
PAT
C3
C5
N
Ca2+
1
2
3
SH3
GK
C
PSD-95
α-actinin
Apo-CaM
Ca2+/CaM

Figure S7. Model of PSD-95 anchoring by α-actinin at postsynaptic sites and its release by Ca^{2+}/CaM upon Ca^{2+} influx, related to Figure 7.

Under basal conditions (left) binding to α-actinin and palmitoylation keeps PSD-95 at postsynaptic sites. Palmitoylation is a prerequisite for postsynaptic localization of PSD-95 and is mediated by palmitoyl acyltransferases (PATs). The PAT DHHC2 is selectively localized at postsynaptic sites to augment PSD-95 palmitoylation and thereby postsynaptic retention although other PATs that are not firmly anchored at postsynaptic sites (e.g., DHHC3) contribute to PSD-95 palmitoylation (Fukata et al., 2013). The α/β-hydrolase domain – containing proteins ABHD17A,B, and C have recently been identified as palmitoyl thioesterases (PPT) that depalmitoylate PSD-95 (Yokoi et al., 2016). Ca^{2+} influx likely stimulates PSD-95 depalmitoylation (El-Husseini et al., 2000), which allows binding of Ca^{2+}/CaM to shift the equilibrium of palmitoylated, α-actinin – bound PSD-95 to non-palmitoylated PSD-95 in part by Ca^{2+}/CaM capping the N-terminus of PSD-95, thereby preventing re-palmitoylation (Zhang et al., 2014). Ca^{2+}/CaM also competes with and thereby displaces α-actinin from the N-terminus of PSD-95 when it is depalmitoylated.

SUPPLEMENTAL TABLES

Table S1. Statistics for Figure 1.

panel	condition	band intensity (AU)	S.E.M
E			
	NT-PDZ-1/2	181.0	30.4
	PDZ2	58.7	17.5
	PDZ3	14.3	6.6
	GK	5.3	2.9
	SH3	22.0	9.0
F			
	MBP	13.4	6.8
	CH1/2	182.1	28.2
	SR1	13.3	8.8
	SR2	31.5	18.5
	SR3	216.0	24.6
	SR4	29.0	4.7
	EF	189.3	36.5
G			
	MBP	11.7	5.2
	CH1	188.5	43.2
	CH2	202.5	40.6
	CH1/2	230.8	15.8
I			
	MBP	9.0	1.1
	EF-ΔPDZ	66.3	11.1
	EF	78.6	13.6

Table S2. Statistics for Figure 2.

panel	condition	puncta / µm	S.E.M	intensity (AU)	S.E.M
A					
		α-actinin (ACTN)			
	vector	0.66	0.06	0.95	0.07
	kd124	0.43	0.05	0.52	0.04
	kd124 + rescue	0.67	0.05	0.76	0.05
	kd3	0.69	0.09	0.86	0.11
		synapsin			
	vector	0.92	0.04	2.21	0.23
	kd124	0.65	0.04	2.33	0.26
	kd124 + rescue	0.99	0.06	2.44	0.30
	kd3	0.89	0.05	2.68	0.33
B					
		PSD-95			
	vector	0.96	0.08	1.8	0.2
	kd124	0.57	0.06	1.1	0.1
	kd124 + rescue	0.88	0.09	1.6	0.1
	kd3	0.93	0.10	1.7	0.2
		GluA1^{EC}			
	vector	0.76	0.06	0.98	0.07
	kd124	0.41	0.05	0.74	0.06
	kd124 + rescue	0.76	0.08	0.95	0.16
	kd3	0.79	0.08	0.94	0.09
C					
		phalloidin			
	vector	0.68	0.07	1.4	0.1
	kd124	0.35	0.03	1.1	0.1
	kd124 + rescue	0.52	0.04	1.6	0.1
	kd3	0.64	0.06	1.5	0.1
D					
		PSD-93			
	vector	0.51	0.05	0.97	0.06
	kd124	0.34	0.03	0.91	0.08
	kd124 + rescue	0.52	0.04	0.94	0.04
	kd3	0.50	0.06	0.86	0.05
		GluA2^{EC}			
	vector	0.47	0.04	0.72	0.03
	kd124	0.32	0.04	0.76	0.04
	kd124 + rescue	0.48	0.05	0.77	0.04
	kd3	0.48	0.05	0.72	0.04
E					
		GluN1^{EC}			
	vector	0.71	0.08	0.91	0.04
	kd124	0.42	0.05	0.95	0.06
	kd124 + rescue	0.70	0.07	0.98	0.05
	kd3	0.75	0.09	1.03	0.04
F					
		SAP102			
	vector	0.90	0.08	0.96	0.05
	kd124	0.21	0.03	0.77	0.06
	kd124 + rescue	0.80	0.07	0.85	0.05
	kd3	0.69	0.07	1.08	0.08
G					
		SAP97			
	vector	0.64	0.09	1.06	0.043
	kd124	0.43	0.07	1.08	0.055
	kd124 + rescue	0.66	0.10	0.97	0.064
	kd3	0.60	0.08	0.88	0.050

Table S3. Statistics for Figure 4.

panel	condition		
B		**expression level (AU)**	**S.E.M**
	RFP	0.312	0.018
	PSD-95^{WT}	0.407	0.019
	PSD-95^{K10E}	0.382	0.036
	PSD-95^{K11E}	0.383	0.023
	PSD-95^{KK10,11EE}	0.378	0.030
C		**synaptic RFP intensity (AU)**	**S.E.M**
	RFP	0.41	0.02
	PSD-95^{WT}	1.00	0.84
	PSD-95^{K10E}	0.74	0.06
	PSD-95^{K11E}	0.71	0.05
	PSD-95^{KK10,11EE}	0.66	0.09
D		**synaptic enrichment factor**	**S.E.M**
	RFP	1.05	0.02
	PSD-95^{WT}	1.77	0.06
	PSD-95^{K10E}	1.57	0.04
	PSD-95^{K11E}	1.48	0.05
	PSD-95^{KK10,11EE}	1.31	0.04

Table S4. Statistics for Figure 5.

panel	condition		
A		**GluA1^{EC} puncta / µm**	**S.E.M**
	RFP	0.021	0.006
	PSD-95^{WT}	0.128	0.021
	PSD-95^{K10E}	0.017	0.004
	PSD-95^{K11E}	0.024	0.008
	PSD-95^{KK10,11EE}	0.028	0.007
		relative synaptic GluA1^{EC} intensity	**S.E.M**
	RFP	0.93	0.06
	PSD-95^{WT}	1.83	0.33
	PSD-95^{K10E}	0.97	0.09
	PSD-95^{K11E}	0.91	0.05
	PSD-95^{KK10,11EE}	1.09	0.08
B		**mEPSC frequency (Hz)**	**S.E.M**
	RFP	0.40	0.15
		2.17	0.24
	PSD-95^{K10E}	0.49	0.21
	PSD-95^{K11E}	0.54	0.13
	PSD-95^{KK10,11EE}	0.64	0.29
		mEPSC amplitude (pA)	**S.E.M.**
	RFP	-5.9	0.3
	PSD-95^{WT}	-11.3	1.2
	PSD-95^{K10E}	-6.4	0.9
	PSD-95^{K11E}	-6.8	0.5
	PSD-95^{KK10,11EE}	-6.9	0.5
		decay time (ms)	**S.E.M.**
	RFP	7.6	0.1
	PSD-95^{WT}	7.5	0.4
	PSD-95^{K10E}	7.6	0.1
	PSD-95^{K11E}	8.1	0.2
	PSD-95^{KK10,11EE}	8.1	0.2
C		**GluN1^{EC} puncta / µm**	**S.E.M**
	RFP	0.20	0.02
	PSD-95^{WT}	0.19	0.03
	PSD-95^{K10E}	0.22	0.03
	PSD-95^{K11E}	0.21	0.03
	PSD-95^{KK10,11EE}	0.20	0.03
		relative synaptic GluA1^{EC} intensity	**S.E.M**
	RFP	1.00	0.04
	PSD-95^{WT}	1.13	0.05
	PSD-95^{K10E}	1.07	0.09
	PSD-95^{K11E}	0.83	0.06
	PSD-95^{KK10,11EE}	0.79	0.07

Table S5. Statistics for Figure 6.

panel	condition		
C		**Spine PSD-95 intensity (AU)**	**S.E.M**
	WT	42.53	4.21
	ED_KK	20.29	1.83
	E53K	20.72	2.12
D		**PSD-95 spine enrichment factor**	**S.E.M**
	WT	5.29	0.59
	ED_KK	2.38	0.15
	E53K	3.13	0.49
E		**GluA2^{EC} spine intensity (AU)**	**S.E.M**
	WT	64.47	5.73
	ED_KK	38.57	2.90
	E53K	33.99	2.18
F		**GluA2^{EC} puncta/µm**	**S.E.M**
	WT	0.51	0.03
	ED_KK	0.29	0.04
	E53K	0.32	0.03
H		**Spine PSD-95 intensity (AU)**	**S.E.M**
	WT	21.70	3.90
	K10E	8.86	0.98
	K11E	10.35	0.96
I		**PSD-95 spine enrichment factor**	**S.E.M**
	WT	4.80	0.40
	K10E	2.05	0.14
	K11E	2.55	0.21
J		**GluA2^{EC} spine intensity (AU)**	**S.E.M**
	WT	33.70	4.67
	K10E	19.98	1.46
	K11E	18.81	1.29
K		**GluA2^{EC} puncta/µm**	**S.E.M**
	WT	0.71	0.04
	K10E	0.48	0.03
	K11E	0.52	0.04

Table S6. Statistics for Figure 7.

panel	condition		
B		**Signal ratio %**	**S.E.M**
	No treatment	97.84	8.98
	NMDA	19.84	3.72
	CMZ+NMDA	96.83	7.12
	W7+NMDA	100.00	7.94
	TFP +NMDA	94.33	10.67
C		**Signal ratio %**	**S.E.M**
	No treatment	100.01	19.88
	NMDA	257.14	37.12
	CMZ+NMDA	96.46	26.96
	W7+NMDA	96.43	18.56
	TFP +NMDA	92.86	27.89

Table S7. Fluorescent stainings performed in the present study.

channel / staining	405 nm	488 nm	555 nm	647 nm
Characterization of α-actinin knock-down				
Figure 2A	synapsin	GFP	α-actinin (EA-53)	bassoon[a]
Figure 2B	PSD-95	GFP	GluA1^{EC}	Shank[a]
Figure 2C	synapsin[a]	GFP	phalloidin	Shank[a]
Figure 2D	synapsin[a]	GFP	GluA2^{EC}	PSD-93
Figure 2E	synapsin[a]	GFP	GluN1^{EC}	bassoon[a]
Figure 2F	synapsin[a]	GFP	SAP102	
Figure 2G	synapsin[a]	GFP	SAP97	
Figure S2		GFP		
Figure S3A	synapsin[a]	GFP	GluN1^{EC}	bassoon
Figure S3B	synapsin[a]	GFP	Phalloidin	Shank
Expression of mutant PSD-95 and α-actinin1				
Figure 4	synapsin[a]	GFP	RFP	
Figure 5A	Shank[a]	GFP	RFP[b]	GluA1^{EC}
Figure 5C	synapsin[a]	GFP	RFP[b]	GluN1^{total}
Figure 6B	α-actinin (Aviva)	GFP	GluA2^{EC}	PSD-95
Figure 6G	MAP2	GFP[c]	GluA2^{EC}	PSD-95
Figure S4	synapsin[a]	GFP	RFP	
Figure S5		GFP		
Figure S6G		phalloidin	DsRed	

[a],[b],[c] Fluorescent signals to identify synaptic sites ([a]) and neurons expressing RFP-PSD-95 ([b]) or PSD-95-GFP ([c]) without being depicted.